

Bridging EUV and white-light observations using the *PROBA2/SWAP* imager and MLSO/MK4 coronagraph via advanced image processing methods: a two-stage eruptive event case study.

J. P. Byrne¹ · et al.

© Springer •••

Abstract Methods of multiscale image analysis were employed and their efficacy on the SWAP data tested for revealing CME structure while suppressing other features. The methods use successive filtering of an image via a Gaussian and derivative-of-Gaussian produces a number of scales of detail to be inspected. This also produces an image with intensities that represent the relative edge strengths in the original image, which can be used to characterize the structure of interest – specifically for this case the erupting material involved in the CME. In order to overlap the observations from SWAP and MK4, the core material of the CME in its early eruption phase was chosen for its higher signal to noise ratio than the CME front, for example, that was not discernible in the early stages of the observations. In the LASCO field-of-view, the core material was determined to be moving at the same speed as the CME front, at $\sim 500 \text{ km s}^{-1}$. The front portion of the core material in the MK4 images was characterized via point-&-click methodology on the multiscale images of enhanced edges, and an ellipse was fit to the curved front. The same was done for the erupting loop structure observed in SWAP, with the expectation that it might directly correlate to the CME core. However, it was found that the erupting material that starts at the same time and location in both the MK4 and SWAP images, did not proceed to erupt at the same rate. Rather the core material observed in MK4 moves at greater speeds than the loop structures observed in SWAP; rising from an initial speed of $\sim 100 \text{ km s}^{-1}$ (at $\sim 1.5 R_{\odot}$) to a final speed of $\sim 400 \text{ km s}^{-1}$ (at $\sim 2 R_{\odot}$), while the loops continue to steadily rise at $\sim 100 \text{ km s}^{-1}$. The reason for this is unclear, and requires further investigation.

Keywords: Coronal Mass Ejections, Initiation and Propagation

¹ Institute for Astronomy, University of Hawai'i, 2680 Woodlawn Drive, Honolulu, HI 96822, USA. email: jbyrne@ifa.hawaii.edu

1. Introduction

Coronal mass ejections (CMEs) represent the largest, most dynamic phenomena that originate from the Sun. Propagating at speeds of hundreds up to thousands of kilometers per second (Yashiro *et al.*, 2004), the particle densities and energies involved can cause adverse space weather at Earth and elsewhere in the heliosphere (Schwenn *et al.*, 2005). They can lead to geomagnetic storms upon impacting our magneto-sphere, damaging satellites, affecting communication and navigation systems, and increasing the radiation risk for astronauts (Lockwood and Hapgood, 2007). Given their potentially hazardous impact on Earth's geomagnetic environment, the physics governing their eruption and propagation needs to be understood.

An important aspect of studying CME initiation, is the ability to resolve their low-corona propagation and associated source regions on the disk: be it a flaring or non-flaring active region, a prominence/filament eruption or other rising loop system, or else a ‘stealth CME’ without any specifically detectable source. Prominence lift-offs often become the core material of a CME, and rising loops often form some part of the CME morphology. Their low-corona kinematics and morphology provide insight into the early forces at play, and so a rigorous study of such phenomena is key to understanding the physics involved.

In order to connect CMEs to their source regions, data from disk imagers such as the Sun Watcher using APS detectors and image Processing (SWAP; Seaton *et al.*, 2013) onboard the second Projects for Onboard Autonomy (*PROBA2*; Santandrea *et al.*, 2013) and the Atmospheric Imaging Assembly (AIA; Lemen *et al.*, 2012) onboard the Solar Dynamics Observatory (*SDO*; Pesnell, Thompson, and Chamberlin, 2012), may be used in tandem with coronagraph observations. However, difficulties in the interpretation of the observed features arise due to the varying instrument specifications, e.g., image passbands, fields-of-view, cadences, etc. Therefore, to bridge the gap between the white-light images of the extended corona and the EUV observations of the solar disk and low corona, the SWAP imager was used in conjunction with the Mauna Loa Solar Observatory (MLSO) MK4 coronagraph (Elmore *et al.*, 2003) to directly compare the observations of CMEs as they erupt through the overlapping fields-of-view (Fig. 1). This allows a direct correspondence of features in the EUV images with those in the white-light images, providing new insight into the connection of CMEs to the Sun during their initial phases of eruption and acceleration away from their source regions on the disk.

A difficulty exists in studies of coronal structure that are prone to low signal-to-noise ratios in the observational data. Low-coronal white-light observations using a coronagraph are problematic due to the strong radial brightness gradient and issues with scattered light in the instrument, while extended EUV disk observations are problematic due to the strong drop-off in emission brightness with increasing coronal height. These common issues with solar observational data motivate the development and use of advanced image processing techniques to suppress noise and enhance structures in the image data (Druckmüllerová, Morgan, and Habbal, 2011, Gallagher *et al.*, 2011, Pérez-Suárez *et al.*, 2011, Stenborg, Vourlidas, and Howard, 2008, Young and Gallagher, 2008, Morgan, Habbal, and Woo, 2006, Stenborg and Cobelli, 2003).

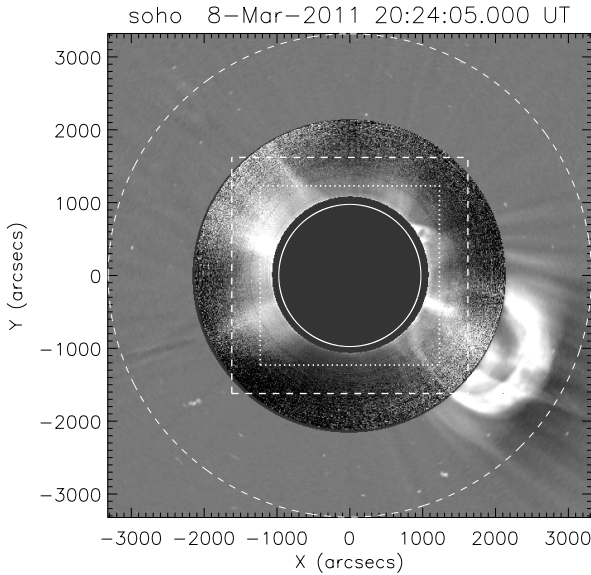


Figure 1. A LASCO/C2 image with an MLSO/MK4 image overlaid in the range $1.1\text{--}2.2 R_{\odot}$, dated 8 March 2011 at 20:24 and 20:22 UT respectively. The C2 image has been processed via the CORIMP techniques of normalizing radial graded filter (NRGF) and quiescent background subtraction. It has been trimmed to a half-width of $3.4 R_{\odot}$, which is the upper limit of the *PROBA2/SWAP* field-of-view as indicated by the dashed circle. The SWAP field-of-view during nominal operations is indicated by the dashed box. The *SDO/AIA* field-of-view is indicated by the inner dotted box. The limb of the Sun behind the occulter is indicated by the solid white circle. A CME is observed off the south-west limb as a bright loop structure with some inner core material, as seen here in the Thomson-scattered white-light coronagraph images. It is clear how the SWAP and AIA images can be used to bridge CME observations to the low corona and solar disk, for gaining insight to their initiation phase.

2. Observations & Techniques

Methods of multiscale image processing have been developed in recent years for use on coronagraph images to enhance the underlying structure. The fundamental idea behind these methods is to highlight details apparent on different scales within the data. Therefore, multiscale techniques provide an ability to remove small-scale features in images, essentially suppressing the noise such that the structures of interest can be revealed in greater detail. By applying them to coronagraph images, the morphology of CMEs as they propagate through the corona in a sequence of observations can be determined with better accuracy than previously possible (Byrne *et al.*, 2009, 2012).

These methods are now demonstrated for use on the MK4 coronagraph and SWAP EUV imager, to provide insight to the low-coronal morphology of erupting structures that may form CMEs. Details on the fundamental technique are outlined in Young and Gallagher (2008) wherein the magnitude of the multiscale gradient is used to show the relative strength of the detected edges in the image structure at a particular scale of the multiscale decomposition (i.e., the strongest edges appear brightest). To increase the signal-to-noise ratio of the edge detec-

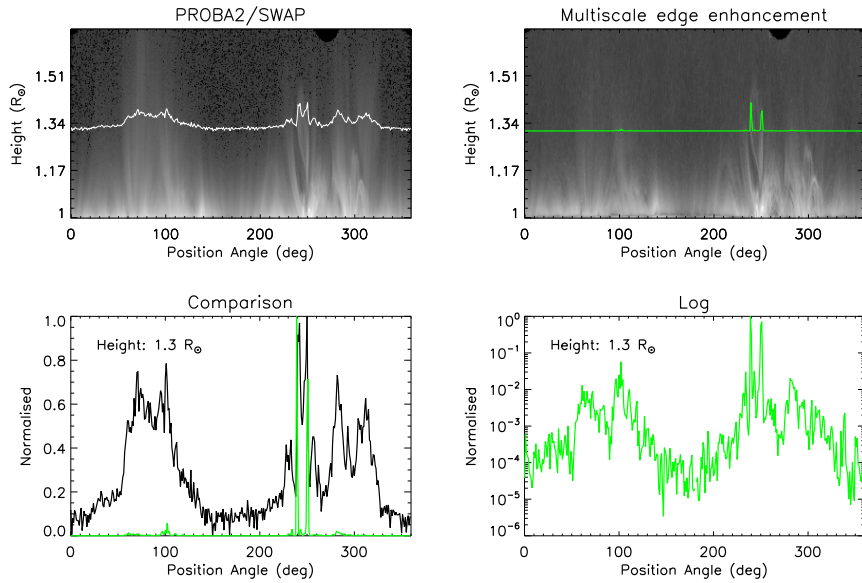


Figure 2. The top two panels show polar-unwrapped images of the solar corona across the *PROBA2/SWAP* field-of-view on 8 March 2011 at 19:53:59 UT; left being the level-1 data, right being the enhanced data. Across each image, at a constant height of $1.3 R_\odot$, an intensity slice is plotted (of arbitrary normalised units) to demonstrate how the background coronal structure is suppressed by the multiscale techniques, to highlight only the complex structure of the prominence. The bottom left plot shows a direct comparison of the two intensity slices, where the prominence is located between $230 - 260^\circ$. The bottom right plot shows a log scale of the normalised intensity slice across the enhanced image to demonstrate that the rest of the coronal structure is still present, just strongly suppressed relative to the prominence material.

tions further, the magnitude information from the scales most relevant to the coronal structures of interest may be multiplied together, neglecting the largest scales that smooth out the coronal signal, and the smallest scales that reveal the finer structure and noise (see Byrne *et al.*, 2012, for details). Thus the magnitude of the multiscale gradient across the dominant edges of coronal loops and CMEs is further enhanced for subsequent characterization of their morphology.

Figure 2 shows the effectiveness of the multiscale techniques for detecting the structure of an ejection observed by SWAP at 19:53:59 UT on 8 March 2011. The top left image shows the level-1 processed data, polar-unwrapped about Sun-center at coronal heights of $1 - 1.7 R_\odot$. The top right image shows the result of the multiscale filtering technique applied in such a manner as to enhance the edges of the detected structure in the data. The bottom left plot shows the comparison of an intensity slice at a height of $1.3 R_\odot$ in each, revealing how the multiscale techniques best characterize the complex structure of the erupting prominence material. While the bottom right plot shows a log of the intensity slice across the multiscale filtered image to reveal the suppressed signal of the background features.

The extended corona from $\sim 2 - 30 R_\odot$ is often observed with the Large Angle Spectrometric Coronagraph (LASCO; Brueckner *et al.*, 1995) onboard the

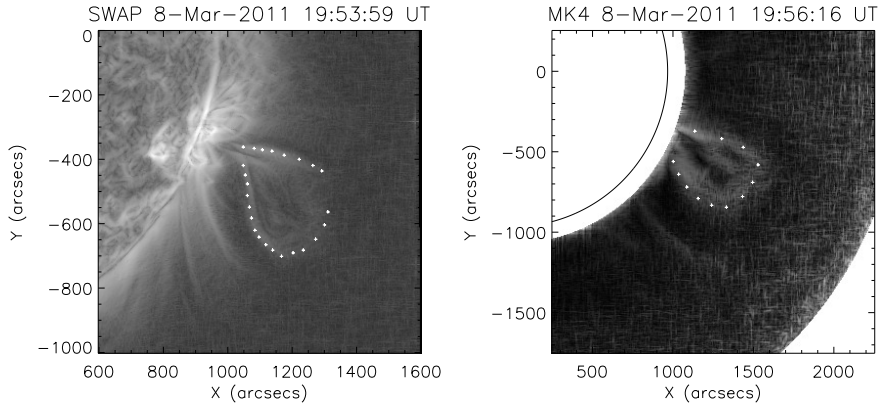


Figure 3. SWAP (left) and MK4 (right) observations of the erupting loop system that forms the inner core of the CME on 8 March 2011, at times 19:52 and 19:53 UT respectively. The images have been processed via the multiscale decomposition, showing here intensities that represent the magnitude of the detected edges.

Solar and Heliospheric Observatory (SOHO; Domingo, Fleck, and Poland, 1995) situated about the L1 point. (Along with the more recently launched SECCHI coronagraphs onboard the STEREO mission, from increasing angles of separation in their orbits about the Sun.) Coronal structures, and specifically CMEs, have been studied in the white-light image data from these instruments through the use of a number of steps outlined in the Coronal Image Processing package (CORIMP; Morgan, Byrne, and Habbal, 2012, Byrne *et al.*, 2012). These techniques have now been extended for use on the MLSO/MK4 coronagraph data, which provides white-light polarization brightness images of the corona from $\sim 1.14 - 2.86 R_{\odot}$. The MK4 data is prepared via an instrumental vignetting function that maximizes the image contrast by offsetting the radial brightness gradient in order to best reveal structures such as CMEs and streamers. A multi-scale decomposition is then performed, in order to produce magnitude images of the relative edge strengths in the image to highlight the detected structure (see Fig. 3). This allows, for example, an ellipse-fit characterization of the outward propagating fronts, as described in Byrne *et al.* (2009).

3. ‘Double Eruption’ of the 8 March 2011 CME

A CME erupted from active region NOAA 11165 (S20W91) at approximately 19:30 UT on 8 March 2011. The active region caused numerous flares during its evolution across the disk, notably an M1.5 flare at GOES start-time 19:35 UT associated with the rising loop system that erupted to form the core material of the CME. The loop system evolution is clearly visible up to $\sim 1.3 R_{\odot}$ in AIA images, at which height a set of loops that are most strongly observed in AIA-171Å images begin to erupt, being observable to a height of $\sim 1.6 R_{\odot}$ in the larger field-of-view of the SWAP-174Å imager. The CME core is then observed in the

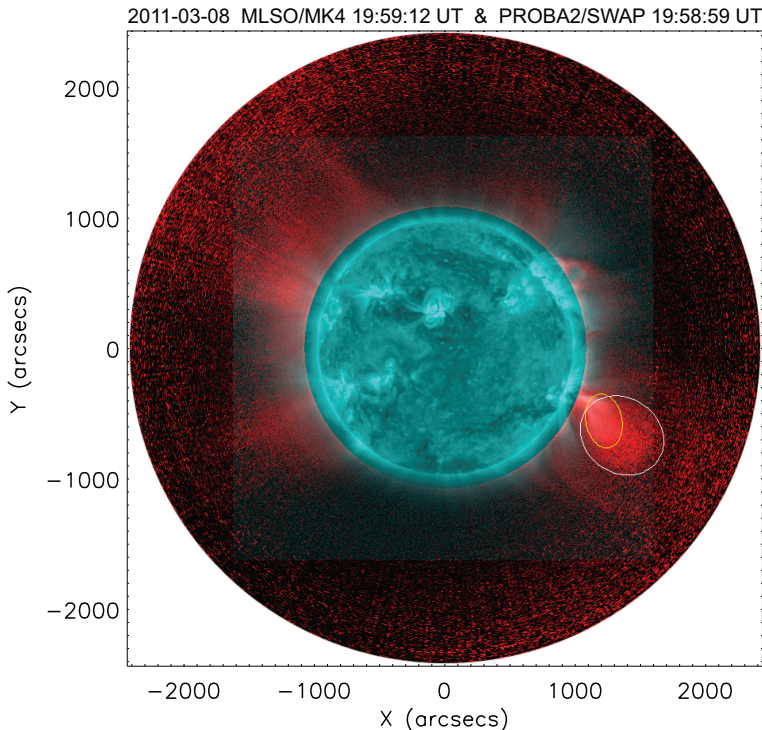


Figure 4. A merged SWAP (blue) and MK4 (red) image with the ellipse fits to the characterized CME core material as observed by each instrument.

white-light MK4 coronagraph images to a height of $\sim 2.2 R_{\odot}$, entrained within a very faint CME bubble that appears to form at these heights before being clearly observed to propagate outwards in the extended LASCO coronagraph images.

Morgan, Jeska, and Leonard (2013) report on the expansion of active region loops from this region into the extended solar corona in the day or so leading up to this CME. The region lies beneath a helmet streamer structure that appears to contain the observed coronal loops, with a number of faint brightenings due to small outward-propagating plasma blobs. These and the pointed shape of the rising loops are postulated to be indicators of helmet streamer interchange reconnection at the apex of the closed field (Wang *et al.*, 2012). A subsequent brightening and expanding of the loops accompanied by a swelling of the helmet streamer, precedes the CME from this region and is evidence for an energy input to the system that leads to an explosive energy release. Such a process manifests as the two-stage solar eruptive event outlined in these and Su *et al.* (2012)'s observational studies.

In order to best reveal the eruption material in the low signal-to-noise SWAP and MK4 images, multiscale methods of noise suppression and edge enhancement were employed, as discussed above. This allowed a robust point-&-click characterization of the core material of the CME, which was the brightest structure to be tracked through the different imagers when the CME front was not yet fully

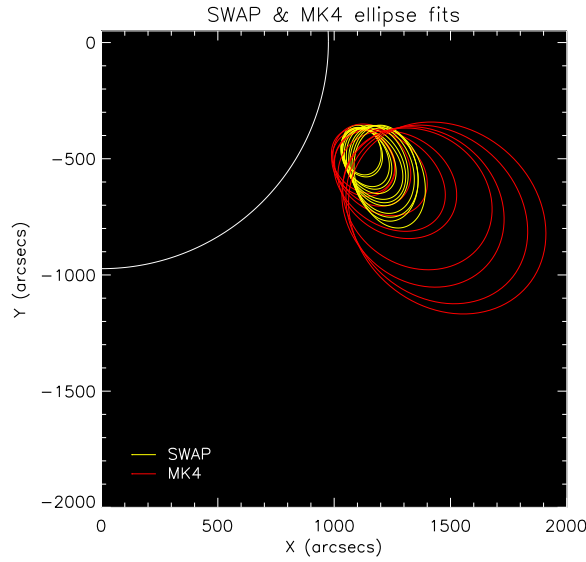


Figure 5. The SWAP and MK4 ellipse fits to the characterized CME core material over the course of the eruption.

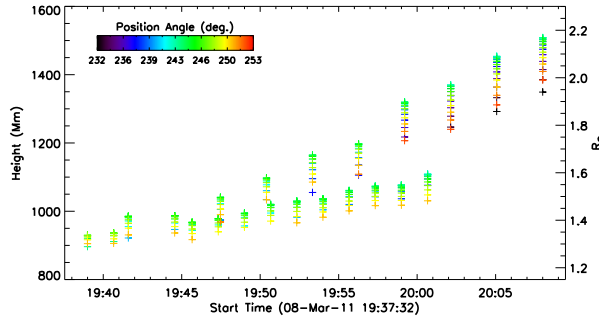


Figure 6. The height-time profile of the characterized eruption observed simultaneously with the SWAP imager and MK4 coronagraph (see the ellipse-fits in Fig. 5 above). The erupting EUV loops move at a speed of $\sim 100 \text{ km s}^{-1}$ while the associated core of the resulting CME is observed to accelerate up to a speed of $\sim 400 \text{ km s}^{-1}$.

formed (Fig. 3). The rising loop system observed with SWAP and the erupting CME core material observed with MK4 coincided both temporally and spatially with each other, at least initially, and each was characterized by ellipse-fits to the detected front edges of the structures. Figure 4 shows an overlay of SWAP and MK4 images during the eruption at times 19:58:59 and 19:59:12 UT respectively, with the ellipses fit to the erupting fronts (from point-&-click characterizations of the edge enhanced multiscale decompositions of the images, as demonstrated in Fig. 3). Figure 5 shows the progression of the ellipse fits to the fronts over the course of the eruption, indicating how the white-light material observed with MK4 propagates away from the source quicker than the EUV material observed with SWAP. The different height-time profiles of the SWAP and MK4 observa-

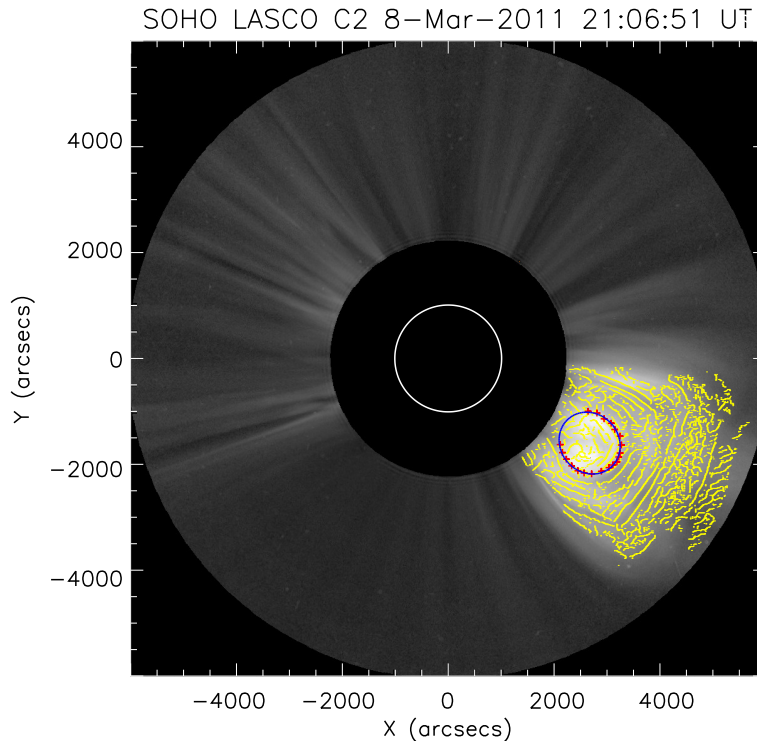


Figure 7. A radially filtered LASCO/C2 image of the CME at 21:06:51 UT on 8 March 2011. The yellow contours trace the edges in the detected CME structure, with red points clicked along the corresponding core material, and a resulting ellipse-fit in blue.

tions are shown in Fig. 6, where the material in the MK4 images attains a speed in the range $400-600\text{ km s}^{-1}$, while the associated erupting loop structures in the SWAP images proceed at only $\sim 100\text{ km s}^{-1}$. The reasons for this are unclear, but the analysis of Su *et al.* (2012) shows that the active region underwent a two-stage flaring process at the time of the eruption that is evidence of a secondary heating phase that coincides with the CME acceleration (Fig. 8).

The CME onset was observed as a series of rising loops, that attained an initial steady height in the low corona of approximately half a solar radii, before destabilizing and becoming the inner core material of a typical three-part CME that propagated out through the corona at a bulk speed of $\sim 400 \text{ km s}^{-1}$, and an initial acceleration of $\sim 20 \text{ m s}^{-2}$ (based on the kinematics of the CME front as detected and tracked in the CORIMP catalog⁴). The core of the CME was manually tracked via the multiscale methods and ellipse-fit discussed above (Fig. 7), and the resulting kinematics are plotted in Fig. 8. The height-time measurements of the CME core are shown in color (corresponding to the position angle of the measurements across the plane-of-sky) overlaid on the CME front height-time measurements shown in gray for reference. The Savitzky-Golay filter is used to

¹<http://dublin.ifa.hawaii.edu/~jbyrne/CORIMP/>

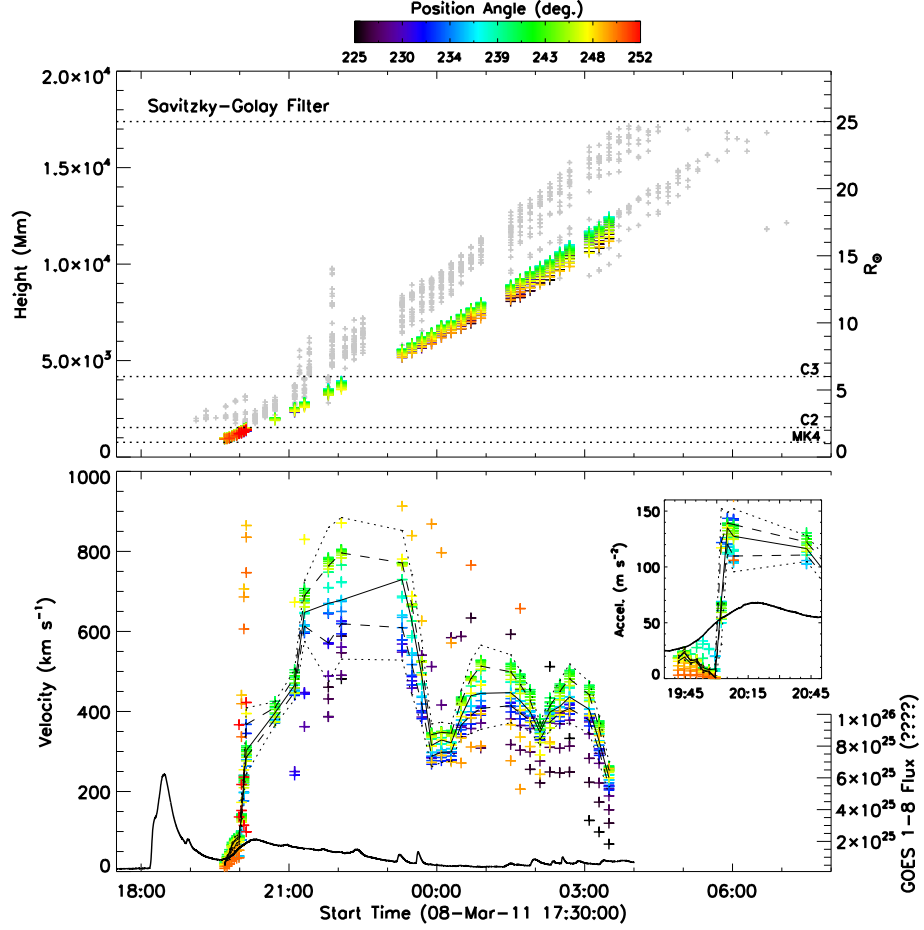


Figure 8. The kinematic profiles of height, velocity, and (inset) the early acceleration phase of the CME core material, detected and characterized via the multiscale edge enhancement and ellipse-fits (see Section 2 and Figs. 5 and 7). The automated CORIMP CME detections provide the height-time measurements shown here in gray for reference, with the characterized CME core height-time measurements plotted in color according to their position angle. The fields-of-view of the MK4, C2 and C3 instruments are indicated by the horizontal dotted lines, covering a useable range of $1.1 - 25 R_\odot$, with the CME core tracked to approximately $18 R_\odot$. A Savitzky-Golay filter was applied to the height-time measurements to obtain distribution profiles of velocity and acceleration, with the median, interquartiles range, and upper/lower fences over-plotted in solid, dashed and dotted lines respectively. Overlaid is the GOES X-ray 1–8 Å flux profile, showing the double-eruption peaks at about 18:30 and 20:15 UT, the latter of which underlies the CME jerk (jump in acceleration).

derive the velocity and acceleration profiles for the CME core (see Byrne *et al.*, 2013 for a detailed discussion). A distribution of velocity and acceleration values is obtained at each data point, with the corresponding median, interquartile range, and upper and lower fences overlaid on each profile as solid, dashed and

dotted lines respectively. The inset acceleration phase of the CME core shows initial values of approximately $\sim 20 \text{ m s}^{-2}$ jumping to $\sim 130 \text{ m s}^{-2}$, which is in agreement with the acceleration profile of the CME front ahead of it. This is not an instrumental effect since it occurs within the MK4 field-of-view before the measurements move into the C2 field-of-view. The abrupt increase in CME acceleration, referred to as the CME jerk by Schrijver *et al.* (2008), is an indication of a very fast energy release that allows the explosive eruption of the CME to begin before attaining a speed akin to the local solar wind speed. This double acceleration profile is further evidence of the complexity of this active region whose morphology has been observed to change dramatically over the course of its evolution (Morgan, Jeska, and Leonard, 2013; Su *et al.*, 2012).

4. Conclusions

The *PROBA2/SWAP* imager is unique in that it provides extended EUV observations of the Sun and low-corona to greater heights than other EUV imagers such as *SDO/AIA*. An ongoing goal in solar physics has been to study the connection between processes on the Sun and the effects felt elsewhere in the heliosphere; a connection known to lie predominantly within the regions of the photosphere, chromosphere and corona. Therefore obtaining and bridging observations across the solar atmosphere is paramount to understanding the physics at play. Since the LASCO/C1 coronagraph was lost very early on in the *SOHO* mission, observations of the low corona have generally been quite limited. In order to bridge this gap and garner some knowledge of the low-corona initiation phase of CMEs, we have combined the SWAP observations with those of the ground-based MK4 coronagraph, to directly compare the EUV and white-light imagery. This was achieved through the use of advanced image processing techniques to overcome the low signal-to-noise ratio in these data, and characterize the erupting structures of interest. The subsequent investigation of the dynamics of a specific case-study provides insight to the early CME formation and eruption, that compliments the previous investigation of Su *et al.* (2012) who first reported on the event's two-stage flaring profile as evidence for secondary heating.

The study of this particular event is of interest in the context of the flare-CME relationship. Firstly, the two-stage flaring profile of the erupting loop system is evidence for a secondary heating process, indicating two stages of magnetic reconnection that occur to first change the topology of the system and then allow for the subsequent flux-rope eruption. This scenario demonstrates that a loss of stability occurs initially, to allow the loop system to rise and alter its magnetic configuration with an explosive energy release detected as an M1.5 flare. This is then followed by a secondary energy release that allows the underlying flux-rope of the system to erupt through the corona as a CME, with the production of a second X-ray peak and post-flare loops at the CME footpoints.

There remain a number of open questions on this event. Firstly, there is no clear explanation for the different rates of motion of the material observed by the SWAP and MK4 instruments during the CME onset (Fig. 6). The simplest reason

is possibly that the material observed by the different instruments corresponds to different parts of the erupting structure that are difficult to dissociate from each other on the plane-of-sky. This could mean that line-of-sight effects are causing a discrepancy in the height-time profiles that appears as this offset in their rates of propagation. Similarly the different parts of the structure may indeed undergo different rates of propagation, and the trailing part either becomes a different portion of the main CME and/or undergoes a delayed jerk in its motion which is not observed with the coverage of these instruments. Alternatively, when we refer to

Acknowledgements This work is supported by SHINE grant 0962716 and NASA grants NNX08AJ07G and NNX13AG11G to the Institute for Astronomy. SWAP is a project of the Centre Spatial de Liège and the Royal Observatory of Belgium funded by the Belgian Federal Science Policy Office (BELSPO). MK4 data is provided courtesy of the Mauna Loa Solar Observatory, operated by the High Altitude Observatory, as part of the National Center for Atmospheric Research (NCAR). NCAR is supported by the National Science Foundation. The *SOHO/LASCO* data used here are produced by a consortium of the Naval Research Laboratory (USA), Max-Planck-Institut fuer Aeronomie (Germany), Laboratoire d'Astronomie (France), and the University of Birmingham (UK). SOHO is a project of international cooperation between ESA and NASA. *SDO* data supplied courtesy of the NASA/*SDO* consortia.

References

- Brueckner, G.E., Howard, R.A., Koomen, M.J., Korendyke, C.M., Michels, D.J., Moses, J.D., Socker, D.G., Dere, K.P., Lamy, P.L., Llebaria, A., Bout, M.V., Schwenn, R., Simnett, G.M., Bedford, D.K., Eyles, C.J.: 1995, The Large Angle Spectroscopic Coronagraph (LASCO). *Solar Physics* **162**, 357–402. doi:10.1007/BF00733434.
- Byrne, J.P., Gallagher, P.T., McAteer, R.T.J., Young, C.A.: 2009, The kinematics of coronal mass ejections using multiscale methods. *Astronomy & Astrophysics* **495**, 325–334. doi:10.1051/0004-6361:200809811.
- Byrne, J.P., Morgan, H., Habbal, S.R., Gallagher, P.T.: 2012, Automatic Detection and Tracking of Coronal Mass Ejections. II. Multiscale Filtering of Coronagraph Images. *Astrophysical Journal* **752**, 145. doi:10.1088/0004-637X/752/2/145.
- Byrne, J.P., Long, D.M., Gallagher, P.T., Bloomfield, D.S., Maloney, S.A., McAteer, R.T.J., Morgan, H., Habbal, S.R.: 2013, Improved methods for determining the kinematics of coronal mass ejections and coronal waves. *Astronomy & Astrophysics* **557**, A96. doi:10.1051/0004-6361/201321223.
- Domingo, V., Fleck, B., Poland, A.I.: 1995, The SOHO Mission: an Overview. *Solar Physics* **162**, 1–2. doi:10.1007/BF00733425.
- Druckmüllerová, H., Morgan, H., Habbal, S.R.: 2011, Enhancing Coronal Structures with the Fourier Normalizing-radial-graded Filter. *Astrophysical Journal* **737**, 88. doi:10.1088/0004-637X/737/2/88.
- Elmore, D.F., Burkepile, J.T., Darnell, J.A., Lecinski, A.R., Stanger, A.L.: 2003, Calibration of a ground-based solar coronal polarimeter. In: Fineschi, S. (ed.) *Society of Photo-Optical Instrumentation Engineers (SPIE) Conference Series, Society of Photo-Optical Instrumentation Engineers (SPIE) Conference Series* **4843**, 66–75. doi:10.1117/12.459279.
- Gallagher, P.T., Young, C.A., Byrne, J.P., McAteer, R.T.J.: 2011, Coronal mass ejection detection using wavelets, curvelets and ridgelets: Applications for space weather monitoring. *Advances in Space Research* **47**, 2118–2126. doi:10.1016/j.asr.2010.03.028.
- Lemen, J.R., Title, A.M., Akin, D.J., Boerner, P.F., Chou, C., Drake, J.F., Duncan, D.W., Edwards, C.G., Friedlaender, F.M., Heyman, G.F., Hurlburt, N.E., Katz, N.L., Kushner, G.D., Levay, M., Lindgren, R.W., Mathur, D.P., McFeaters, E.L., Mitchell, S., Rehse, R.A., Schrijver, C.J., Springer, L.A., Stern, R.A., Tarbell, T.D., Wuelser, J.-P., Wolfson, C.J., Yanari, C., Bookbinder, J.A., Cheimets, P.N., Caldwell, D., Deluca, E.E., Gates, R., Golub, L., Park, S., Podgorski, W.A., Bush, R.I., Scherrer, P.H., Gummin, M.A., Smith, P., Auker, G., Jerram, P., Pool, P., Soufli, R., Windt, D.L., Beardsley, S., Clapp, M., Lang,

- J., Waltham, N.: 2012, The Atmospheric Imaging Assembly (AIA) on the Solar Dynamics Observatory (SDO). *Solar Physics* **275**, 17–40. doi:10.1007/s11207-011-9776-8.
- Lockwood, M., Hapgood, M.: 2007, The Rough Guide to the Moon and Mars. *Astronomy and Geophysics* **48**(6), 060000–6. doi:10.1111/j.1468-4004.2007.48611.x.
- Morgan, H., Byrne, J.P., Habbal, S.R.: 2012, Automatically Detecting and Tracking Coronal Mass Ejections. I. Separation of Dynamic and Quiescent Components in Coronagraph Images. *Astrophysical Journal* **752**, 144. doi:10.1088/0004-637X/752/2/144.
- Morgan, H., Habbal, S.R., Woo, R.: 2006, The Depiction of Coronal Structure in White-Light Images. *Solar Physics* **236**, 263–272. doi:10.1007/s11207-006-0113-6.
- Morgan, H., Jeska, L., Leonard, D.: 2013, The Expansion of Active Regions into the Extended Solar Corona. *Astrophysical Journal Supplement* **206**, 19. doi:10.1088/0067-0049/206/2/19.
- Pérez-Suárez, D., Higgins, P.A., Bloomfield, D.S., McAteer, R.T.J., Krista, L.D., Byrne, J.P., Gallagher, P.T.: 2011, “Automated Solar Feature Detection for Space Weather Applications”, in *Applied Signal and Image Processing: Multidisciplinary Advancements*, eds. R. Qahwaji, R. Green, & E. L. Hines, (IGI Global), p. 207–225.
- Pesnell, W.D., Thompson, B.J., Chamberlin, P.C.: 2012, The Solar Dynamics Observatory (SDO). *Solar Physics* **275**, 3–15. doi:10.1007/s11207-011-9841-3.
- Santandrea, S., Gantois, K., Strauch, K., Teston, F., Tilmans, E., Baijot, C., Gerrits, D., De Groof, A., Schwehm, G., Zender, J.: 2013, PROBA2: Mission and Spacecraft Overview. *Solar Physics* **286**, 5–19. doi:10.1007/s11207-013-0289-5.
- Schrijver, C.J., Elmore, C., Kliem, B., Török, T., Title, A.M.: 2008, Observations and Modeling of the Early Acceleration Phase of Erupting Filaments Involved in Coronal Mass Ejections. *Astrophysical Journal* **674**, 586–595. doi:10.1086/524294.
- Schwenn, R., dal Lago, A., Huttunen, E., Gonzalez, W.D.: 2005, The association of coronal mass ejections with their effects near the Earth. *Annales Geophysicae* **23**, 1033–1059.
- Seaton, D.B., Berghmans, D., Nicula, B., Halain, J.-P., De Groof, A., Thibert, T., Bloomfield, D.S., Raftery, C.L., Gallagher, P.T., Auchère, F., Defise, J.-M., D’Huys, E., Lecat, J.-H., Mazy, E., Rochus, P., Rossi, L., Schühle, U., Slemzin, V., Yalim, M.S., Zender, J.: 2013, The SWAP EUV Imaging Telescope Part I: Instrument Overview and Pre-Flight Testing. *Solar Physics* **286**, 43–65. doi:10.1007/s11207-012-0114-6.
- Stenborg, G., Cobelli, P.J.: 2003, A wavelet packets equalization technique to reveal the multiple spatial-scale nature of coronal structures. *Astronomy & Astrophysics* **398**, 1185–1193. doi:10.1051/0004-6361:20021687.
- Stenborg, G., Vourlidas, A., Howard, R.A.: 2008, A Fresh View of the Extreme-Ultraviolet Corona from the Application of a New Image-Processing Technique. *Astrophysical Journal* **674**, 1201–1206. doi:10.1086/525556.
- Su, Y., Dennis, B.R., Holman, G.D., Wang, T., Chamberlin, P.C., Savage, S., Veronig, A.: 2012, Observations of a Two-stage Solar Eruptive Event (SEE): Evidence for Secondary Heating. *Astrophysical Journal Letters* **746**, L5. doi:10.1088/2041-8205/746/1/L5.
- Wang, Y.-M., Grappin, R., Robbrecht, E., Sheeley, N.R. Jr.: 2012, On the Nature of the Solar Wind from Coronal Pseudostreamers. *Astrophysical Journal* **749**, 182. doi:10.1088/0004-637X/749/2/182.
- Yashiro, S., Gopalswamy, N., Michalek, G., St. Cyr, O.C., Plunkett, S.P., Rich, N.B., Howard, R.A.: 2004, A catalog of white light coronal mass ejections observed by the SOHO spacecraft. *Journal of Geophysical Research (Space Physics)* **109**, 7105. doi:10.1029/2003JA010282.
- Young, C.A., Gallagher, P.T.: 2008, Multiscale Edge Detection in the Corona. *Solar Physics* **248**, 457–469. doi:10.1007/s11207-008-9177-9.